# ASSESSMENT OF CHARGE STATE AND HYDROGEN UTILIZATION OF FUEL CELL ELECTRIC VEHICLE IN DRIVING CYCLE

## M. Rahli    A. Chaker

*SCAMRE Laboratory, Department of Electrical Engineering, National Polytechnic School of Oran - Maurice Audin (ENPO-MA), Oran, Algeria, mehdi.rahli@enp-oran.dz, chakeraa@yahoo.fr*

**Abstract-** This paper aims to analyze and study the management of energy flows in a hybrid system made up of two sources: a PEMFC-type fuel cell and a battery (Li-ion) as auxiliary. A DC/DC converter regulates the fuel cell's output voltage before mixing with the battery, which delivers power to the drive motor. the synchronous permanent magnet motor produces the motive Force necessary to propel the wheels; where energy is routed through the transmission shaft and differential, containing all devices in addition to vehicle form, was created using MATLAB/Simulink. A model of power management has been built into the system so that the output power changes under different conditions. We determined an efficiency estimation of the consumption of hydrogen and a charge state of the Li-ion battery at any time value by using fitting formulas. The vehicle operating modes closely match the proposed power system for supervision. Furthermore, the hybrid percentage is valued to assess overall efficiency. Obtained results show little relationship with the efficacy.

**Keywords:** Electric Vehicle, Fuel Cell, Lithium Ion, Bi-Directional Converter, Energy Management.

## 1. INTRODUCTION

Vehicles with internal combustion engines are essential in everyday life because they save considerable time, but with all technological successes, we have realized that these vehicles contribute greatly to global warming thanks to the harmful gases emitted from their exhaust. After much research, an interesting alternative has appeared, electric vehicles (Replacement of the heat engine by another electric one), which are zero-emission vehicles, and hybrid electric vehicles (HEV), the quantities of gases such as CO, $CO_2$, and Nox are in very small quantities.

For a long autonomous of these 100% electric vehicles, batteries necessity to be charged since they will be exhausted [1]. This generates disadvantages compared to usual cars which have a long autonomous drive, and also a high cost of recharging. Thus, to resolve these problems, researchers have designed hybrid vehicles such as fuel cell vehicles (FCV), resulting in a very long autonomous drive compared to 100% electric cars.

The main element for better functioning of the FCV is certainly a fuel cell which provides additional power to the electric vehicle so that it can reach or even surpass the autonomy of a gasoline or diesel cars.

## 2. FUEL CELL VEHICLE

A fuel cell vehicle can be considered as a series HEV using hydrogen as the alternative fuel. Electricity for both the on-board batteries and the electric motor is supplied by the fuel cell that works like the generator in series HEVs [2]. Fuel cell vehicles are the promising technology for they can eliminate the environment pollution from vehicles completely. Among its innumerable advantages, a fuel cell generates electricity thanks to the already known principle which is the reverse of the water electrolysis. The control system is shown in Figure 1 [3].
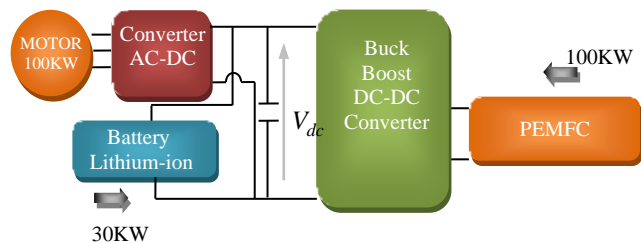


Figure 1. Control system of the FCV [3]

In Figure 2, the forces that oppose the vehicle movement are: the force which opposes the rolling $F_{tire}$, this is due to the rubbing of the tires on the road; any subject which travels in the air is the seat of the aerodynamic drag force $F_{aero}$. Finally, if the vehicle is moving on a slope, there will be an opposite climb force $F_{slope}$ [4-6].
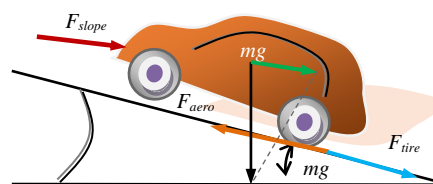


Figure 2. Control system of the FCV [5]

By summing all the mentioned forces, we arrive at the force $F_r$ in Equation (1) [5].

$$F_r = F_{tire} + F_{aero} + F_{slope} \qquad (1)$$

where,

$$F_{tire} = mgf_r \qquad (2)$$

$$F_{aero} = \frac{1}{2} p_{air} A_f C_d v^2 \qquad (3)$$

$$F_{slope} = mg \sin(\beta) \qquad (4)$$

All FCV parameters are cited in Table 1 [7].

Table 1. Electric vehicle's parameters

| | |
|---|---|
| $r$ | 0.26 m |
| $m$ | 1625 Kg |
| $f_r$ | 0.01 |
| $A_f$ | 2.711 m$^2$ |
| $C_d$ | 0.26 |
| $P_{air}$ | 1.2 Kg/m$^3$ |

## 2.1. PEMFC Operation Principle

The main reaction in a PEMFC is [8-11].

$$H_2 + \frac{1}{2} O_2 \rightarrow H_2O + Heat + Electrical energy \qquad (5)$$

Through this reaction, and in addition to water and heat, an electrical energy is produced. The membrane separates the oxidation of hydrogen and the reduction of oxygen and it sends the protons from the negative electrode (anode) to the positive electrode (cathode) to obtain an electric current, The semi-reactions on the two electrodes are [10]:

$$H_2 \rightarrow 2H^+ + 2e^- \ Anode \qquad (6)$$

$$O_2 + 4e^- \rightarrow 2O_2 + Cathode \qquad (7)$$

The electrical circuit transports electrons in which their energy can be used while protons are being transported across the membrane. Fuel cell modeling is of great interest to scientists in the field of power electronics, because a greatest number of fuel cell stacks, depending on their powers [6]. Jefferson M. Correa presented a PEMFC model which is built on the simulation of the association between the output voltage and current in one hand, and on the other the hydrogen's partial pressure and respectively oxygen. The basic scheme of the PEMFC is shown in Figure 3 [10].

$$V_{cell} = E_{ac} - E_{act} - E_{conc} + E_{ohmic} \qquad (8)$$

$$E_{act} = \frac{RT}{2aF} \ln(\frac{i}{i_0}) \qquad (9)$$

$$E_{conc} = \frac{RT}{2F} \ln(\frac{i_L}{i_L - i}) \qquad (10)$$

$$E_{ohmic} = R_\Omega i \qquad (11)$$

In order to obtain a higher voltage in operating, the cells are connected in series and in case of having a stack PEM consisting of $N$ cells [6]. The stack voltage is given by Equation (12):

$$V_{stack} = NV_{cell} = N(E - E_{act} - E_{conc} - E_{ohmic}) \qquad (12)$$

Parameters of the above equations that have been used for the simulation model appear in the Appendices.
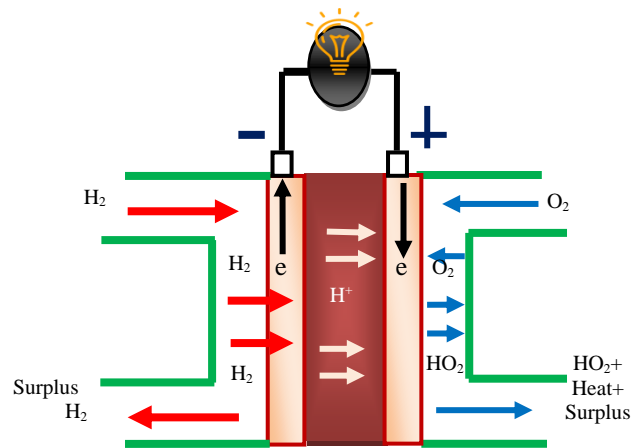


Figure 3. PEMFC Principle [6]

## 2.2. Permanent Magnet Synchronous Motor

The EV (or the HEV) works with a salient rotor PMSM (with characteristics $V = 288$ V, $P = 100$ KW, and number of poles = 8) with the association of a drive. Thanks to flux vector control, the maximum motor speed can reach 12,500 rpm. The PMSM is widely used since it offers many advantages over other competitors (especially the induction motor). Maintenance of a PMSM is very easy, this will ensure higher operating efficiency. If one is in front of high powers or low speed loads, the PMSM is best suited for direct drive [12-15].

## 2.3. DC-DC Converter

A DC/DC voltage converter is used for adjusting the battery low voltage (200 V) to the DC bus to then supply the motor of the HEV. Depending on the use, the converter can be used in BOOST (to increase the operating voltage) or a BUCK converter (to reduce the operating voltage) [16-18].

## 2.4. Operation Principle of Lithium-Ion Battery

Li-ion technology consists of passing electrons by generating a voltage drop between the two electrodes, (which are always of opposite sign), which are in contact with an ionic liquid which is conductive (the electrolyte) [19-21].



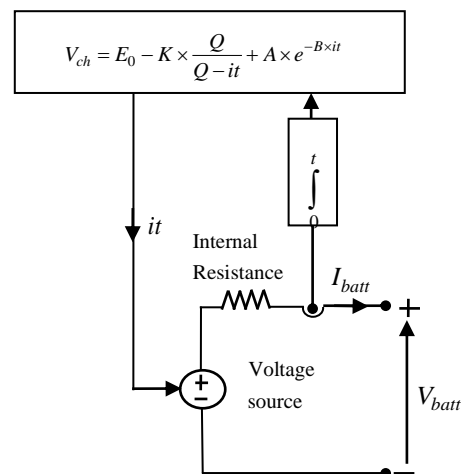$$V_{ch} = E_0 - K \times \frac{Q}{Q - it} + A \times e^{-B \times it}$$

Figure 4. Equivalent circuit of a lithium-ion battery [20]

When the battery powers a device, the electrons collected in the NE are released through an external circuit until they reach the PE: this is the discharge interval. when the battery begins to charge, the energy transmitted by the charger causes a reinstatement from electrons to the NP to the NE [20]. Figure 4 describes the equivalent circuit of a Lithium-ion battery.

## 3. SIMULATION RESULTS

Simulations are divided into four modes from the FCV operation over a complete cycle: acceleration, displacement, recharge phase by accelerating and slowing down by recovery, all details are illustrated in Figures 5 and 6.
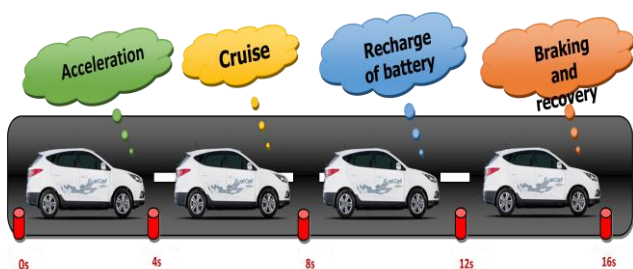


Figure 5. Different scenarios of electric vehicle
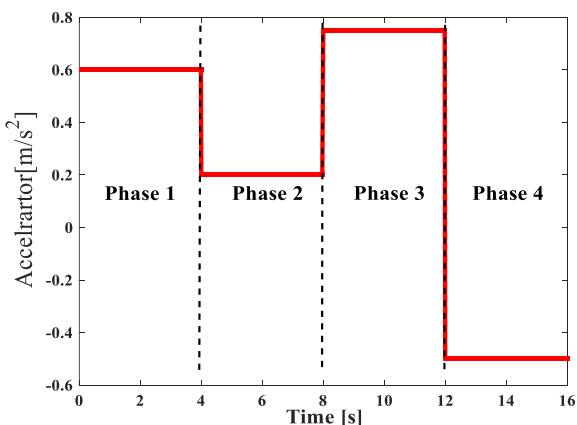


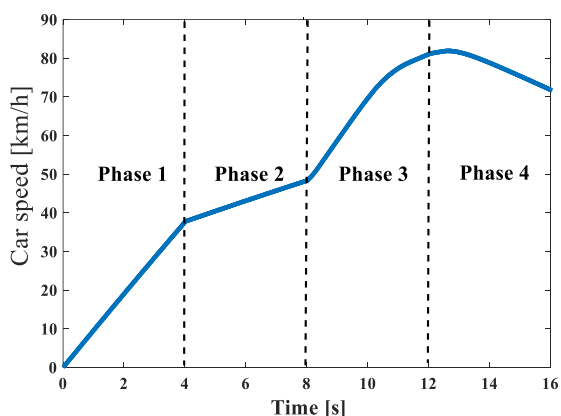Figure 6. Accelerating and travelling for all FCV modes



Figure 7. FCV speed for one cycle

From Figure 7, at first the vehicle speed begins by 0 km/h to almost 80 km/h, the time is 12 s; then a speed reduction to 70 km/h well time is 16 s.

This is achieved by belonging the acceleration at 60% for the first fourth seconds and at 20% for the next fourth seconds once the pedal is let out, next at 75% although the pedal is pressed once more for fourth seconds and in the end at -50% (decelerating) till the simulation finish.
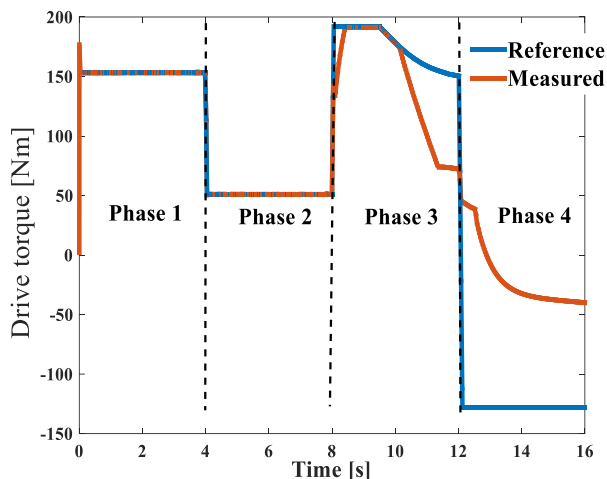


Figure 8. Driving and electromagnetic torque variation during a day

At $t = 0$ s, the torque setpoint is set to 178 Nm (the nominal torque of the motor is 256). The electromagnetic torque quickly reaches the reference. At $t = 4$ s, the electromagnetic torque decreases to the value of 50 Nm in the second phase. Accordingly, a flux attenuation is affected so as to limit the counter electromotive force of the engine; Therefore, the current component $I_d$ is increased (negatively). In addition, the reference torque is limited (due to torque-speed characteristics) to prevent saturation of the inverter, which causes a decrease in the current component $I_q$. Note that the amplitude of the current is constant; Only the angle changes.
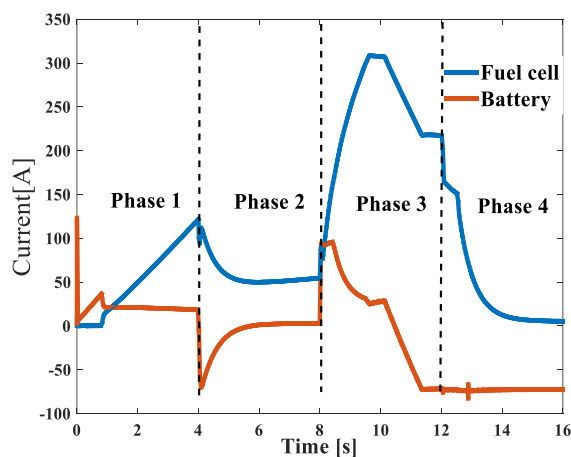


Figure 9. Variation of current of fuel cell and battery

Signals of reference for the electric motor are determined by the EMS, a system of fuel cell and a DC/DC converter have the role of precisely distributing the power from both sources. Negative throttle location means the brake is in the positive position.
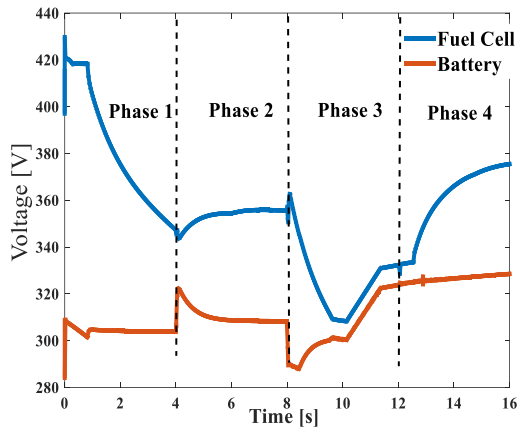
Figure 10. Variation of voltage of fuel cell and battery

The management system of battery reserves the right to keep the SOC between 40 and 80%. Moreover, and through the control of the necessary power of the battery it prevents the collapse of the voltage. This system examines the electric motor baseline power by dividing the power according to this last existing from fuel cell and the battery. the role of the DC/DC converter is to control this power.

### 3.1. Fuel Cell Results

From Figure 11 note that the air flow reaches 2000 liters per minute when the FCV reaches a speed of 75 km/h and the hydrogen flow and 500 lpm (third phases), while the flow of air reaches 500 lpm when the speed of the FCV is a little near 60 km/h, it can be concluded that the air flow increases as the speed increases. The use of oxygen and hydrogen during the different scenarios is shown in Figure 17. The voltage, current of PEMFC and its performance throughout the FCV path is illustrated in Figure 11.
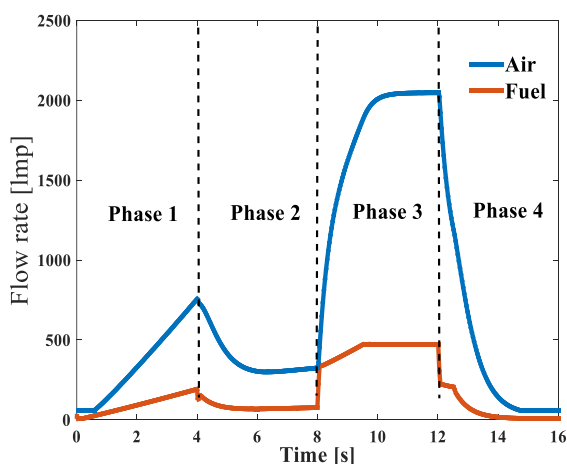


Figure 11. Air and Oxygen flow of the PEMFC during different cases

Hydrogen consumption is 120 lpm during the second phase, it reaches 400 lpm during the lithium-ion battery recharging phase and tends towards zero during the energy recovery phase.
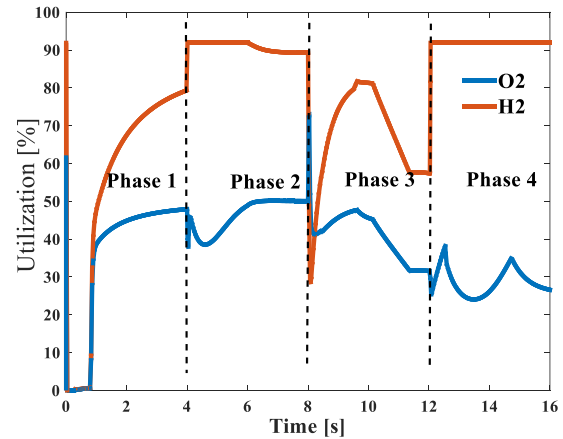


Figure 12. Use of oxygen and hydrogen of PEMFC during different cases

### 3.2. Fitting Formulas

### 3.2.1. Fitting Formula for Air Consumption

$$Y = 8.5 \times 10^{-5} x^9 - 0.66 \times 10^{-2} x^8 + 0.21 x^7 - $$
$$-3.6 x^6 + 35 x^5 - 1.9 \times 10^2 x^4 + 5.6 \times 10^2 x^3 - $$
$$-8 \times 10^2 x^2 + 5.3 \times 10^2 x - 84$$

### 3.2.2. Fitting Formula for Fuel Consumption

$$Y = 3.6 \times 10^{-5} x^9 - 0.28 \times 10^{-2} x^8 + 0.089 x^7 - $$
$$-1.5 x^6 + 15 x^5 - 80 x^4 + 2.4 \times 10^2 x^3 - $$
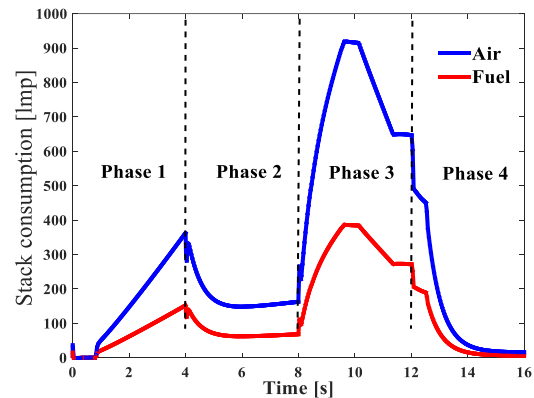$$-3.4 \times 10^2 x^2 + 2.2 \times 10^2 x - 35$$



Figure 13. Consumption of oxygen and hydrogen of the PEMFC during different cases

The variation of the efficiency of the PEMFC during the whole path of the FCV is illustrated in Figure 14. The average Flow rate, Stack consumption and Utilization for fuel cell in different scenarios are shown in Table 2.

### 3.3. Lithium-Ion Battery Results

When the SOC of the battery falls below 40% on the $t = 10.9$ s (it was initially set at 40.32% just at commencement of the simulation), the battery should be charged up. The power generated by the fuel cell is shared by the motor and the battery. It is easy to see how the battery power depletes, this is because the fuel cell powers the battery which begins to recharge when the FCV accelerates, as shown in Figure 16.
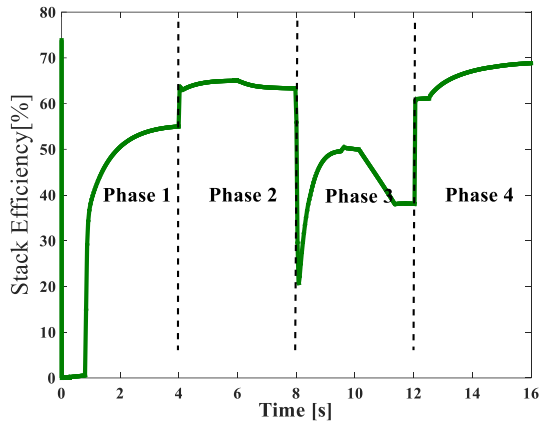
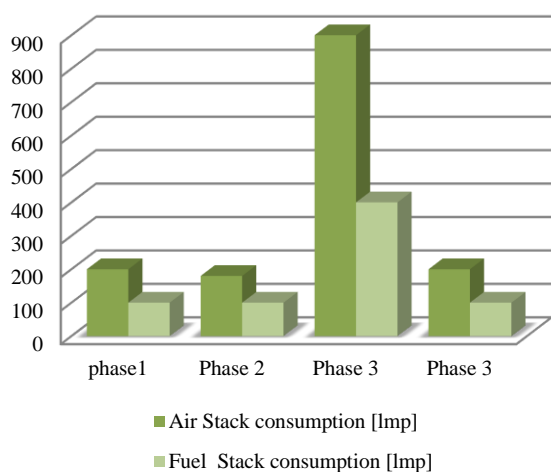Figure 14. Stack Efficiency of the PEMFC during different cases



Figure 15. Histogram of stack consumption in different phases

Table 2. Average flow rate, stack consumption and utilization for fuel cell

|  | Phase1 | Phase 2 | Phase 3 | Phase 4 |
|---|---|---|---|---|
| Air Flow rate [lmp] | 100 | 350 | 2000 | 1000 |
| Fuel Flow rate [lmp] | 400 | 100 | 500 | 500 |
| Stack Efficiency [%] | 40 | 65 | 50 | 70 |
| Utilization $O_2$ [%] | 45 | 50 | 45 | 30 |
| Utilization $H_2$ [%] | 70 | 90 | 75 | 90 |

Table 3. States of charging battery for each end of cycle

| Time [s] | 0 | 4 | 8 | 12 | 16 |
|---|---|---|---|---|---|
| State of charge [%] | 40.32 | 40.11 | 40.18 | 40.22 | 40.79 |

### 3.3.1. Fitting Formula for State of Charge

$$Y = 1.8 \times 10^{-7} x^8 - 10^{-5} x^7 + 0.23 \times 10^{-3} x^6 -$$

$$-0.25 \times 10^{-2} x^5 + 0.13 \times 10^{-1} x^4 - 0.3 \times 10^{-1} x^3 +$$

$$+0.18 \times 10^{-1} x^2 - 0.33 \times 10^{-1} x + 40$$

### 3.4. Power Results

When the FCV stops on the $t = 0$ s, the pilot depresses the accelerator to 60%. The motor is powered by the battery till the fuel cell begins to function on the $t = 0.7$ s, power is provided by fuel cell without achieving the reference power (This is because of the design where the constant time is large). The battery still powers the motor. on the $t = 4$ s, the driver releases the accelerator to 20%.
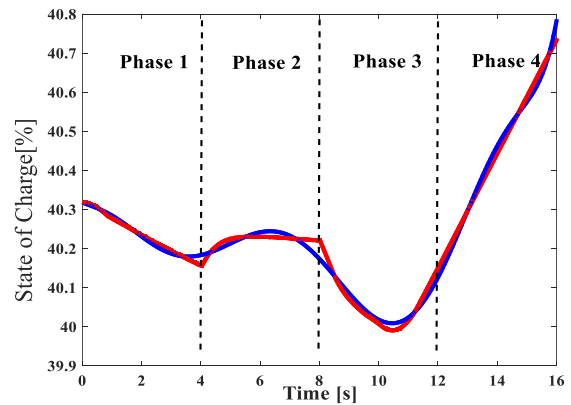


Figure 16. Variation of charge state of battery during different phases

The power of fuel cell begins to gradually decrease; therefore, the battery absorbs this power so that the requested torque is maintained. on the $t = 6$ s, the power of fuel cell has reached the reference level. The battery intervention is not compulsory, it can be seen in Figure 17. For $t = 8$ s, the accelerator goes to 75%. At this time the battery provides an additional power of 25 kW to help the fuel cell. At $t = 8.05$ s, the two added powers cannot reach the required energy (as already mentioned, the response time of a fuel cell is quite long.). Therefore, the measured driving torque cannot reach that of the reference

For The measured torque reference is obtained on the $t = 8.45$ s. As the power of the fuel cell increases, the battery power gradually decreases to 6 kW. On $t = 12$ s, the accelerator pedal is at -50% (at this time we simulate the regenerative braking). The wheels of the vehicle drive the motor (the latter acts as a generator).

The battery stores electrical energy, this energy comes from the transformation of the FCV kinetic energy. Because of battery can only get 25 kW of energy, the needed torque of -140 Nm cannot be achieved for this pedal position. (Figure 3). The power of fuel cell is reduced depending on the response. on the $t = 15$ s, power of fuel cell reaches almost 2 kW (the least power).
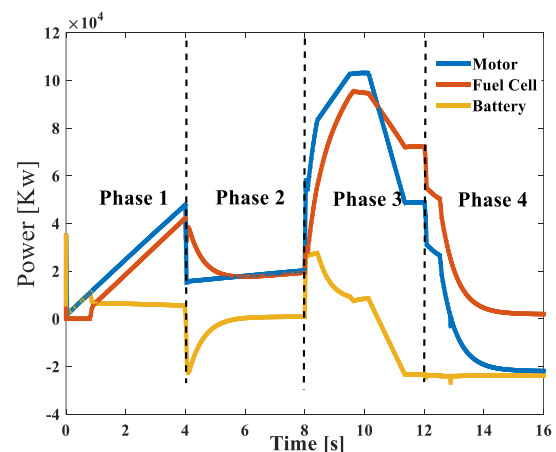


Figure 17. Powers variation of different sources thus motor during different phases

## 4. CONCLUSIONS

In this paper, an HEV fuel cell model was presented and used for the purpose of analyzing dynamic power and performance delivery. All simulations were run by MATLAB/Simulink software to assess the driving cycle and overall fuel efficiency of the HEV. The study covers several driving scenarios. From the results obtained, it can be concluded that:

1) The HEV is power-driven by two power sources connected in parallel, simultaneously. To compensate for the power deficit of the PEMFC, a Li-ion battery is added. The additional energy supplied is stored in the PEMFC.

2) For testing driving cycle, we used ECE40 acceleration instructions. Thus, and through the proposed control strategy obtained results justify good driving vehicle.

## APPENDICES

### Appendix 1. PMSM Parameters

Table 4. PMSM Parameters [20]

| Nominal voltage (line-line) [V] | 380 |
|---|---|
| Nominal power [KW] | 15 |
| Stator resistance per phase[$\Omega$] | 0.0083 |
| Direct stator inductance $L_d$ [mH] | 0.17415845761 |
| Quadrature inductance of stator $L_q$ [mH] | 0.292668882377 |
| Magnets established Flux [V.s] | 51.5954 |
| Inertia J [Kg.m$^2$] | 0.102 |
| Friction factor [Nm/s] | 0.009541 |
| Pole pairs | 4 |

### Appendix 2. Battery Parameters

Table 5. Battery parameters [20]

| Nominal voltage [V] | 288 |
|---|---|
| Capacity [Ah] | 13.9 |
| Maximum capacity [Ah] | 13.9 |
| Initial charge state [%] | 40.32 |
| Voltage at full charge[V] | 335.2283 |
| Rated discharge current[A] | 6.0435 |
| Internal resistance[$\Omega$] | 0.20719 |

### Appendix 3. PEMFC Parameters

Table 6. PEMFC parameters [10]

| Nominal stack power [KW] | 85.5 |
|---|---|
| Maximum stack power [KW] | 100 |
| Fuel cell resistance [$\Omega$] | 0.17572 |
| Nominal utilization: Hydrogen (H$_2$) [%] Oxidant (O$_2$) [%] | 95.24 50.03 |
| Nominal consumption: Fuel [slpm] Air [slpm] | 794.4 1891 |
| Current Exchange [A] | 0.024152 |
| Exchange coefficient [alpha] | 1.1912 |

### Appendix 4. Variation of Fuel Cell Signal Parameters

Table 7. Fuel cell signal variation parameters [11]

| Fuel cell compositions ($x$-H$_2$) [%] | 99.95 |
|---|---|
| Oxidant composition ($y$-O$_2$) [%] | 21 |

| Rate of Fuel flow (Fuel Fr) at nominal hydrogen utilization [lpm] | 374.8 |
|---|---|
| Rate of Fuel flow (Fuel Fr) at maximum hydrogen utilization [lpm] | 456.7 |
| Air flow (Air Fr) at nominal oxidant utilization[lpm] | 1698 |
| Air flow (Air Fr) at Maximum oxidant utilization[lpm] | 2069 |
| System temperature [°K] | 368 |
| Pressure Fuel cell pressure (PFuel) [bar] | 3 |
| Pressure of Air cell (PAir) [bar] | 3 |

## NOMENCLATURE

### 1. Acronyms

PEMFC     Proton Exchange Membrane Fuel Cell
HEV     Hybrid Electric Vehicle
EV     Electric Vehicle
PMSM     Permanent Magnet Synchronous Motor
FCV     Fuel cell Vehicle
NE     Negative electrode
PE     Positive electrode
EMS     Energy Management System
SOC     State of charge

### 2. Symbols / Parameters

$F_r$: The total resistive force
$F_{tire}$: The rolling resistance force
$F_{aer}$: The aerodynamic resistance torques
$V_{cell}$: The output voltage for a single cell
$V_{stack}$: The stack voltage for $N$ cells
$E_{oc}$: The open circuit PEMFC voltage
$E_{act}$: The voltage drop caused by the activation losses
$E_{conc}$: The voltage drop caused by the concentration losses
$E_{ohmic}$: The voltage drop caused by the ohmic losses
$R$: The ideal gas constant
$T$: The cell temperature
$F$: The Faraday Constant
$i_0$: The current density of reference exchange
$i_L$: The current density limits
$R_\Omega$: The ohmic resistance of the membrane
$\alpha$: The transfer coefficient
$V_{ch}$: The nonlinear voltage
$Q$: The maximum battery capacity (Ah)
$E_0$: The constant voltage
$K$: The polarization constant (Ah$^{-1}$)
$A$: The exponential voltage (V)
$B$: The exponential capacity
$it$: The extracted capacity

## REFERENCES

[1] I.J.M. Besselink, P.F. van Oorschot, E. Meinders, H. Nijmeijer, "Design of an Efficient, Low Weight Battery Electric Vehicle Based on a VW Lupo 3L", The 25th World Battery, Hybrid and Fuel Cell Electric Vehicle Symposium and Exhibition Shenzhen, China, 5-9 November 2010.

[2] E. Demirkutlu, I. Iskender, "Three-Phase Buck Type PFC Rectifier for Electrical Vehicle Battery Charger", International Journal on Technical and Physical Problems of Engineering (IJTPE), Issue 41, Vol. 11, No. 4, pp. 51-56, December 2019.

[3] N.J. English, R.K. Shah, "Technology Status and Design Overview of a Hybrid Fuel Cell Engine for A

Motorcycle", Second International Conference on Fuel Cell Science, Engineering and Technology, FuelCell2004, No. 2457, June 2004.

[4] A.A. Abd El Monem, M.A. Ahmed, S.A. Mahmoud, "Dynamic Modelling of Proton Exchange Membrane Fuel Cells for Electric Vehicle Applications", Journal of Petroleum and Environmental Biotechnology, ISSN 2157-7463, Issue 2, Vol. 5, 2014.

[5] G. Brahim, C. Abdelkader, A. Laoufi, B. Alloua, "Adaptive Fuzzy PI of Double Wheeled Electric Vehicle Drive Controlled by Direct Torque Control", Leonardo Electronic Journal of Practices and Technologies, ISSN 1583-1078, Issue 17, pp. 27-46, July-December 2010.

[6] A.C. Farcas, P. Dobra, "Adaptive Control of Membrane Conductivity of PEM Fuel Cell", The 7th International Conference Interdisciplinarity in Engineering, Procedia Technology, Petru Maior University, Vol. 12, pp. 42-49, Targu Mures, Transylvania, Romania, 2014.

[7] B. Arnet, L.P. Haines, "Combining Ultra-Capacitors with Lead-Acid Batteries", The 17th International Electric Vehicle Symposium and Exposition, Montreal, QC, Canada, 15-18 October 2000.

[8] A. Burke, "Electrochemical Capacitors for Electric Vehicles, Technology Update and Implementation Considerations", The 12th International Electric Vehicle Symposium (EVS-12), University of California at Davis, Vol. 1, Sessions 1A-2D, pp. 27-36, California, USA, 1994.

[9] A. Burke, "Ultracapacitors: Why, How, and Where is the Technology", Journal of Power Sources, Issue 1, Vol. 91, pp. 37-50, January 2000.

[10] N. Mebarki, T. Rekioua, Z. Mokrani, D. Rekioua, S. Bachab, "PEM Fuel Cell/ Battery Storage System Supplying Electric Vehicle", International Journal of Hydrogen Energy, Issue 45, Vol. 41, pp. 20993-21005, 7 December 2016,

[11] F. Caricchi, F. Crescimbini, F.G. Capponi, L. Solero, "Ultracapacitors Employment in Supply Systems for EV Motor Drives: Theoretical Study and Experimental Results", The 14th Electric Vehicle Symposium, University of Rome, Italy, 1997.

[12] S. Delprat, T.M. Guerra, J. Rimaux, "Optimal Control of a Parallel Power Train: from Global Optimization to Real Time Control Strategy", Vehicular Technology Conference, The 55th Vehicular Technology Conference, Birmingham, AL, USA, 06-09 May 2002.

[13] J.W. Dixon, M. Ortuzar, E. Wiechmann, "Regenerative Braking for an Electric Vehicle using Ultracapacitors and a Buck-Boost Converter", The IEEE Aerospace and Electronic Systems Magazine, Issue 17, Vol. 8, pp. 16-21, September 2002.

[14] S. Rao, B. Bairwa, D. Ahmed, S. Staines, "Regenerative Braking System Using a DC/DC Buck-Boost Converter", Journal of River Publishers, Vol. 9-15, 2021.

[15] J.M.A. Marquez, F.S. Manzano, M.J.V. Vazquez, "A Hybrid Vehicle Configuration with Zero Emission", International Journal of Renewable Energy Technology, Vol. 1, No. 3, March 2005.

[16] G. Paganelli, T.M. Guerra, S. Delprat, Y. Guezennrc, G. Rizzoni, "Optimal Control Theory Applied to Hybrid Fuel Cell Powered Vehicle", IFAC Proceedings Volumes, Issue 1, Vol. 35, pp. 253-258, 2002.

[17] Bheemireddy Thanusha, G. Sujatha, "Modelling and Design of an Electric Vehicle Fed with Dual Drive Motors using Hybrid Energy Storage System", International Journal of Innovative Technology and Exploring Engineering (IJITEE), Issue 4, Vol. 10, February 2021.

[18] P. Thounthong, S. Rael, B. Davat, I. Sadli, "Control of Fuel Cell/Battery Hybrid Source for Electric Vehicle Applications", The 37th IEEE Annual Power Electronics Specialists Conference, Jeju, South Korea, 18-22 June 2006.

[19] A.R. Sadat, A. Pashaei, S. Tohidi, M.B.B. Sharifian, "A Novel SVM-DTC Method Of IN-WHEEL Switched Reluctance Motor Considering Regenerative Braking Capability in Electric Vehicle", International Journal on Technical and Physical Problems of Engineering (IJTPE), Issue 29, Vol. 8, No. 4, pp. 19-25, December 2016.

[20] I. Chaoufi, O. Abdelkhalek, B. Gasbaoui, "State of Charge Estimation of Lithium-Ion Batteries Using Adaptive Neuro Fuzzy Inference System", The IAES International Journal of Artificial Intelligence (IJ-AI) Vol. 11, No. 2, pp. 473-484, June 2022.

[21] J. Zhang, X. Lu, J. Xue, B. Li, "Regenerative Braking System for Series Hybrid Electric City Bus", The World Electric Vehicle Journal (WEV), Issue 4, Vol. 2, pp. 128-134, 2008.

[22] A.J. Del Real, A. Arce, C. Bordons, "Development and Experimental Validation of a PEM Fuel Cell Dynamic Model", Journal of Power Sources, Issue 1, Vol. 173, pp. 310-324, 8 November 2007.

## BIOGRAPHIES

**Mehdi Rahli** was born in Mascara, Algeria on September 7, 1989. He received the B.Sc. degree in 2010 and the M.Sc. degree in Electronics from University of Oran, Oran, Algeria, in 2012. Currently, he is a Ph.D. student at Electrical Engineering Department, ENPO-MA, Oran, Algeria. He is a member of "SCAMRE" laboratory. His research interests are in Electric vehicles, energy management systems, and smart grids.

**Abdelkader Chaker** was born in Oran Algeria, in 1952. He received the Ph.D. degree in electrical engineering from Polytechnic Institute of Saint Petersburg, Russia in 2002. He is a Professor at Electrical Engineering Department, ENPO-MA, Oran, Algeria and director of "SCAMRE" laboratory. His research activities include control of large power systems, multi machine multi converter systems and unified power-flow controllers. His teaching themes are neural process control and real-time simulation of power systems. He is author and co-authors of many scientific publications.